Materials Physics and Mechanics 47 (2021) 978-986
Research article

Received: September 7, 2021
Accepted: September 9, 2021

ON PHYSICAL PROPERTIES OF FEW-PHOTON DETECTORS BASED ON STRUCTURES WITH MICROPILLARS

Dmitriy Tsarev[1], Andrei Bazhenov[1]✉, Maxim Odnoblyudov[2], Alexander Alodjants[1]

[1]Institute of Advanced Data Transfer Systems, ITMO University, St. Petersburg, Russia 197101

[2]Peter the Great St. Petersburg Polytechnic University, St. Petersburg, Russia 195251

✉ b.a.y@mail.ru

Abstract. We develop the model of micropillar photodetectors operated in the infrared domain. The model is based on an algorithm, which uses analytical methods and numerical simulation of Schrödinger equation, aimed at the calculation of the energy levels and wave functions of a semiconductor micropillar. We define the heterostructure as a combination of different semiconductor materials grown one on top of the other via epitaxial methods. The photon-detecting scheme is based on the fact that electrons in potential wells have different energies, and the transition between them (including tunneling) is induced by the absorption of a quantum of energy. The most probable optical transitions are verified; two particular transitions corresponding to the infrared range are demonstrated and relevant photo-current dependencies are discussed.

Keywords: photodetector, micropillar, semiconductor heterostructure

Acknowledgements*. This work was performed by Leading Research Center "National Center of Quantum Internet" of ITMO University during the implementation of the government support program, with the financial support of Ministry of Digital Development, Communications and Mass Media of the Russian Federation and RVC JSC; Grant Agreement ID: 0000000007119P190002, agreement No. 006-20 dated 27.03.2020. Authors are grateful to prof. E.A. Viktorov for useful comments and discussions*.

Citation: Tsarev Dmitriy, Bazhenov Andrei, Odnoblyudov Maxim, Alodjants Alexander. On physical properties of few-photon detectors based on structures with micropillars // Materials Physics and Mechanics. 2021, V. 47. N. 6. P. 978-986. DOI: 10.18149/MPM.4762021_16.

1. Introduction

Nowadays quantum devices operating at single photon level represent a primary interest in photonic quantum technologies [1]. In particular, it is worth mentioning current achievements in quantum cryptography and communication where single photon source, operations, transmission, and efficient detection play a significant role [2,3]. Current quantum information technologies use quantum dots (QDs) to encode and manipulate information embodied in single photons [4]. Micropillars which contain semiconductor quantum dots sandwiched by high-quality DFB-mirrors represent a natural environment for quantum devices operating at low intensity (up to single photon level) design [5-10]. In particular, micropillars with a low number of QDs as a gain medium are profusely used for lasing [11-13], superradiance [14], single-photon emission, which demonstrates high antibunching of

photons [15]. In low dimensions epitaxially grown high-quality planar microcavities provide strong interaction between photonic field and QDs.

On the other hand, one of the promising and well-established technologies of single-photon measurement is based on single-photon avalanche diodes [16].

In this paper, we focus on modeling the physical properties of micropillar systems, which may be capable of single photon measurement in the infrared domain, cf. [17,18]. Our model is based on the Schrödinger equation numerical simulation of semiconductor micropillar microstructure possessing some specific cylindrical geometry containing QDs [19,20]. For calculating the energy levels of complex semiconductor heterostructures we use methods proposed in [21] and widely explored in photodetectors modeling. Semiconductor heterostructure is defined as a combination of different semiconductor materials grown via epitaxial methods. For the calculation, we examine the heterostructure with InAs QDs. The most probable optical transitions are calculated; two particular transitions corresponding to the infrared range are demonstrated. The photon-detecting scheme is based on the fact that electrons in potential wells have different energies, and the transition between them (including tunneling) is induced by the absorption of a quantum of energy. We discuss the resulting photo-current dependency.

2. Two-well model

We consider a micropillar model demonstrated in Fig. 1, cf. [18]. The diameter of the micropillar is D = 256 nm; it is a combination of cylinder-shaped InAs quantum dots with height L_2 = 7 nm and diameter of 43 nm, and an InGaAs quantum well of width L_1 = 10 nm, separated by a thin barrier of $Al_{0.16}Ga_{0.31}In_{0.53}As$ of width d = 3 nm, see Fig. 1(a). This heterostructure with the full-width L = 20 nm is grown over a 150 nm InP substrate. The lower and upper contact layers of n-doped InGaAs are also grown, in order to collect the photocurrent resulting from the photodetection processes.

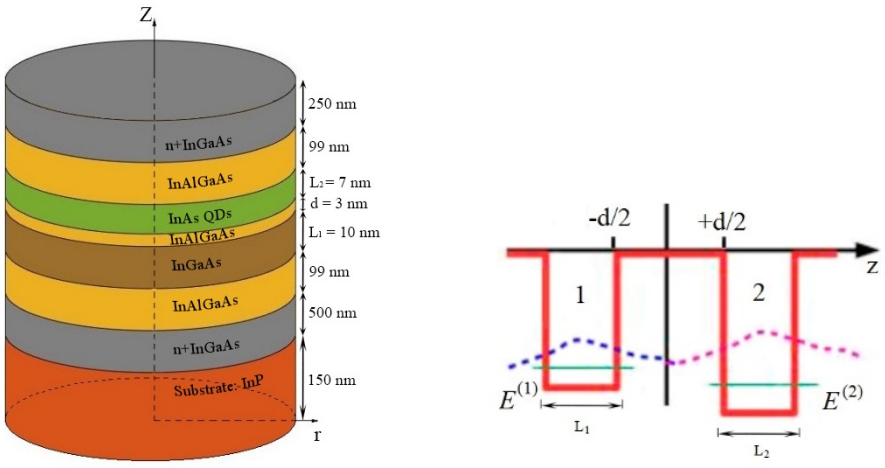

(a) (b)

Fig. 1. (a) Micropillar geometry and heterostructure of a micropillar with quantum dots (QDs); (b) The effective double-well energy profile of the conduction band. Quantum wells possess the widths L_1 = 10 nm and L_2 = 7 nm, they are separated by distance d = 3 nm; the diameter of the micropillar is D = 256 nm [18]

We are interested in the quantum-mechanical calculation of the behavior of the electrons in the conduction band, trapped by effective (double-well) potential V(**r**), shown in Fig. 1(b). The sample geometry provides the cylindrical symmetry of micropillar wave functions Ψ(**r**,t). Schrödinger equation for such a system is written as

$$i\hbar\frac{\partial\Psi(\boldsymbol{r},t)}{\partial t}=\left[-\frac{\hbar^2}{2m_e}\nabla^2+V(\boldsymbol{r})\right]\Psi(\boldsymbol{r},t), \quad (1)$$

and the wave functions obey the normalization condition

$$\int_\Omega|\Psi(\boldsymbol{r},t)|^2d\boldsymbol{r}=N_T, \quad (2)$$

where Ω is the volume of the cylinder of wave function localization, N_T is the number of electrons causing an electric current in the conduction band. For the sake of convenience, we use dimensionless units in (1). For that, we choose characteristic length a_0 = 1 nm and characteristic frequency $\omega_0=\hbar/m_e a_0^2\approx 1.16\times10^{14}$ Hz [22]. Further, all the spatial dimensions are represented in nanometers, and time is given in ω_0^{-1} units if not specified. Particular energy values we will give in electron-volts; in equations, energies are written in $\hbar\,\omega_0$ units, where $\hbar\omega_0\approx 1.22\times10^{-20}$ J = 76.2 meV. Finally, we introduce in (1) the replacement $\Psi'(\boldsymbol{r},t)=a_0^{3/2}\Psi(\boldsymbol{r},t)$ (further we omit the drops for simplicity of notation) to obtain the dimensionless version of Schrödinger equation:

$$i\frac{\partial\Psi(\boldsymbol{r},t)}{\partial t}=\left[-\frac{1}{2}\nabla^2+V(\boldsymbol{r})\right]\Psi(\boldsymbol{r},t). \quad (3)$$

Equation (3) possesses stationary solutions $\Psi_{1,2}(\boldsymbol{r},t)=\Phi_{1,2}(\boldsymbol{r})e^{-iE^{(1,2)}t}$ for the left and right sides of the barrier, respectively, cf. Fig. 1(b); $\Phi_j(\boldsymbol{r})$ describes the spatial distribution of electrons in j-th well, and $E^{(j)}$ specifies their energy levels, respectively.

Substituting these solutions into (3), we obtain the dimensionless equation:

$$\left[-\frac{1}{2}\nabla^2+V(\boldsymbol{r})\right]\Phi_{1,2}(\boldsymbol{r})=E^{(1,2)}\Phi_{1,2}(\boldsymbol{r}). \quad (4)$$

First, consider two isolated quantum wells, when the barrier between them is infinitely high, and the tunneling is negligible. In this case, we can take in (4) $V(\boldsymbol{r})=0$, and write it as

$$-\frac{1}{2}\nabla^2\Phi_{1,2}(\mathbf{r})=\mathrm{E}_{1,2}\Phi_{1,2}(\mathbf{r}), \quad (5)$$

where E_j is the mean energy of the electrons isolated in the j-th well with an infinitely high barrier between the wells. Since the system possesses axial symmetry, we are looking for factorizable solutions of (5) in cylindrical coordinates [23]:

$$\Phi(\boldsymbol{r})=R_{lm}(r)\phi_l(\varphi)Z_n(z), \quad (6)$$

where we omit indices 1 and 2 for simplicity of notation. In Eq. (6) $R_{lm}(r)$, $\phi_l(\varphi)$, and $Z_n(z)$ describe electron wave functions in cylindrical coordinates: r (radius-vector), φ (angle), and z axis, respectively, see Fig. 1(a); n, l, and m are relevant quantum numbers. Substituting (6) into (5) we obtain the set of equations:

$$\frac{\partial^2\phi_l(\varphi)}{\partial\varphi^2}+l^2\phi_l(\varphi)=0; \quad (7a)$$

$$\frac{\partial^2Z_n(z)}{\partial z^2}+(2E-\alpha^2)Z_n(z)=0; \quad (7b)$$

$$\rho^2\frac{\partial^2R_{lm}(\rho)}{\partial\rho^2}+\rho\frac{\partial R_{lm}(\rho)}{\partial\rho}+(\rho^2-l^2)R_{lm}(\rho)=0, \quad (7c)$$

where $\rho=\alpha r$. At the boundaries $\Phi(r=R,\varphi,z)=0$, $\Phi(r,\varphi,z=0,L)=0$ (R and L are the radius of the micropillar and the length of the well, respectively). Therefore, Eqs. (7) admit the following solutions:

$$\phi_l(\varphi)=\frac{1}{\sqrt{2\pi}}e^{il\varphi}; \quad (8a)$$

$$Z_n(z)=\sqrt{\frac{2}{L}}\sin\left[\frac{\pi n}{L}z\right]; \quad (8b)$$

$$R_{lm}(r)=\frac{J_l\left(\frac{k_{lm}r}{R}\right)}{\sqrt{\int_0^R\left|J_l\left(\frac{k_{lm}r}{R}\right)\right|^2dr}}, \quad (8c)$$

where $n=1,2,\ldots$; $l=0,1,\ldots$; and $m=1,2,\ldots$ are the quantum numbers determining the eigenfunctions (6); k_{lm} is the m-th zero of the l-th order first kind Bessel function (this

number can be obtained numerically from the equation $J_l(k_{lm}) = 0$), thus $\alpha \equiv \alpha_{lm} = k_{lm}/R$. Functions (6) are normalized as

$$\int_\Omega |\Psi(\boldsymbol{r}, t)|^2 d\boldsymbol{r} = \delta_{n,n'}\delta_{l,l'}\delta_{m,m'}, \quad (9)$$

and the energy levels (in $\hbar\omega_0$ units) for the *j*-th well ($j = 1,2$) have the form:

$$E_{j,nlm} = \frac{1}{2}\left(\frac{\pi^2}{L^2}n_j^2 + \frac{k_{lm}^2}{R^2}\right). \quad (10)$$

The L parameter characterizes the potential well width; R is the micropillar radius.

Now, taking into account electron tunneling we put $V(\boldsymbol{r}) \neq 0$ in (4). Notice that in the barrier region the modulus of the electron wave functions vanishes exponentially [24]. This allows searching the solutions of (4) in a superposition form:

$$\Psi(\boldsymbol{r}, t) = a_1(t)\Phi_1(\boldsymbol{r} + \boldsymbol{r}_0/2) + a_2(t)\Phi_2(\boldsymbol{r} - \boldsymbol{r}_0/2), \quad (11)$$

where $\Phi_{1,2}(r)$ are wave functions defined in (6) for each of the wells separately; $\boldsymbol{r_0}$ is a vector with components $(0,0,d)$ (d is the distance between the centers of the wells, see Fig. 1(b)); $a_{1,2}(t)$ are time-dependent functions, which define the electric current properties. The solution (11) obey the conditions

$$\int_\Omega \Phi_1^*\Phi_2 d\boldsymbol{r} \simeq 0\,; \quad (12)$$

and from (2) it follows that

$$\int_\Omega \left|\Phi_{1,2}(\boldsymbol{r}, t)\right|^2 d\boldsymbol{r} = \delta_{n,n'}\delta_{l,l'}\delta_{m,m'}\,; \quad (13a)$$

$$|a_1(t)|^2 + |a_2(t)|^2 \equiv N_1(t) + N_2(t) = N_T, \quad (13b)$$

where N_T is defined in (2). Thus, we can recognize $N_1(t)$, $N_2(t)$ as the numbers of particles in the left and right wells, respectively. Substituting (11) with (12) and (13) into (4) we obtain

$$i\frac{\partial a_1}{\partial t} = E^{(1)}a_1 - \kappa a_2; \quad (14a)$$

$$i\frac{\partial a_2}{\partial t} = E^{(2)}a_2 - \kappa a_1, \quad (14b)$$

where

$$E^{(1,2)} = \int_\Omega \left[-\frac{1}{2}\nabla^2\Phi_{1,2} + V\Phi_{1,2}\right]\Phi_{1,2}^* d\boldsymbol{r} = E_{nlm}^{(1,2)} + \int_\Omega V\left|\Phi_{1,2}\right|^2 d\boldsymbol{r}\,; \quad (15a)$$

$$\kappa = -\int_\Omega \left[-\frac{1}{2}\nabla^2\Phi_1 + V\Phi_1\right]\Phi_2^* d\boldsymbol{r}. = -\int_\Omega V\Phi_1\Phi_2^* d\boldsymbol{r}. \quad (15b)$$

Notice that in (15b) in general $\kappa \neq 0$ due to the finite $V(\boldsymbol{r})$ function under the integral. In (15) $E^{(1,2)}$ characterize the energies of electrons in booth wells with the potential correction; κ characterizes the energy of the tunnel coupling (the rate of particle tunneling) between the wells.

Due to the symmetry properties of the micropillar, potential varies only in the z direction, $V(\boldsymbol{r}) \equiv V(z)$; it has three reference points: $V_1 = 240$ meV $\approx 3.15\hbar\omega_0$ and $V_2 = -30$ meV $\approx -0.39\hbar\omega_0$ are the depths of two wells, and $V_0 = 470$ meV $\approx 6.17\hbar\omega_0$ is the height of the potential barrier between them. I.e. the potential has a form (we take the left border of the first well as the coordinate center):

$$V(z) = \begin{cases} V_1, \text{for } 0 \le z < L_1; \\ V_0, \text{for } L_1 \le z < L_1 + d; \\ V_2, \text{for } L_1 + d \le z < L_1 + d + L_2, \end{cases} \quad 16)$$

where $L_1 = 10$ nm and $L_2 = 7$ nm are the widths of the wells and $d = 3$ nm is the distance between them, respectively, see Fig. 2. To calculate κ, we choose an approximation of the rectangular potential (16) using a polynomial:

$$V(z) = V^{(0)}(z) + V^{(1)}(z) + V^{(2)}(z), \quad (17a)$$

where

$$V^{(0)}(z) = \frac{1}{2}[\text{sign}(z - L_1) - \text{sign}(z - L_1 - d)]\left[V_0 - \left(\frac{2\left(z + 0.003\text{ nm} - L_1 - \frac{d}{2}\right)}{d + 0.026\text{ nm}}\right)^{200}\right]; \quad (17b)$$

$$V^{(1)}(z) = \frac{1}{2}[1 - \text{sign}(z - L_1)]\left[V_1 + \left(\frac{2(z-0.055\text{ nm}-L_1)}{L_1+0.11\text{ nm}} + 1\right)^{200}\right]; \quad (17c)$$

$$V^{(2)}(z) = \frac{1}{2}[1 + \text{sign}(z - L_1 - d)]\left[V_2 + \left(\frac{2(z-0.025\text{ nm}-L_1-d)}{L_2+0.05\text{ nm}} - 1\right)^{200}\right], \quad (17d)$$

$\text{sign}(x) = |x|/x = \pm 1$. Notice, one can also apply an external electric field, E_{el}, in the z direction (or equivalently apply the potential difference to the structure) to modify the potential height as $V'(z) = V(z) - E_{el}z$.

Now we can find the energy spectra (15a). Since we are only interested in the strong transitions, we consider only transitions to lower energy levels with $n = 1,2,\ldots,6$; $l = 0,1,2$; $m = 1,2$. We also need to calculate k_{lm}, the m-th zeroes of the l-th order Bessel function, from the condition $J_l(k_{lm}) = 0$; the results are presented in Table 1.

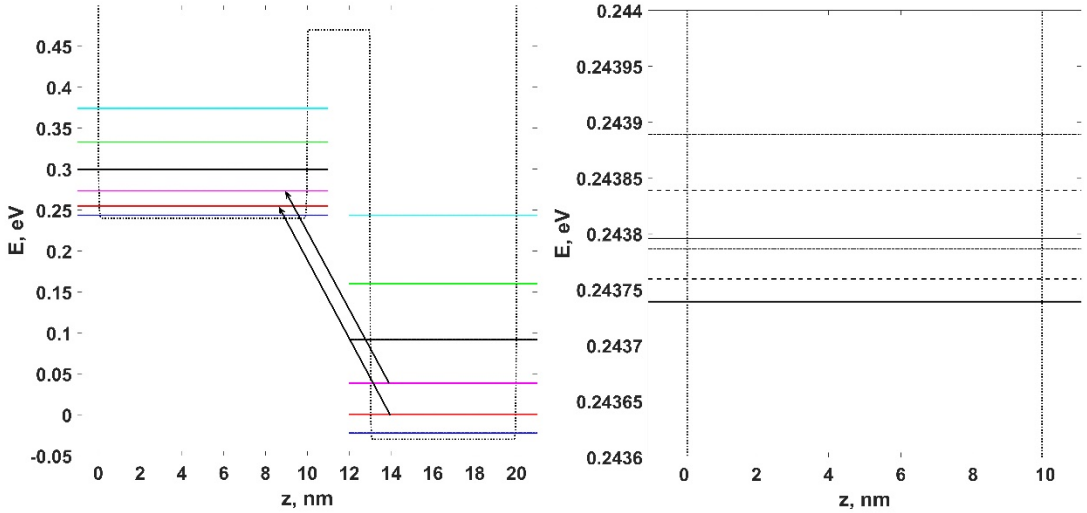

(a) (b)

Fig. 2. (a) Electron energy levels (given in physical units) in two wells; different colors correspond to quantum numbers $n = 1,2,\ldots,6$ in ascending order from bottom to top. The arrows indicate the strongest transitions (see text) (b) Fine structure of the ground energy level of the first well, the solid lines correspond to $l = 0$; dotted – $l = 1$; dashed-and-dotted lines – $l = 2$. The black dotted curve denotes the potential $V(z)$

Table 1. The values of k_{lm}, the m-th zeroes of the l-th order first kind Bessel function

	$l = 0$	$l = 1$	$l = 2$
$m = 1$	$k_{01} = 2.40$	$k_{11} = 3.83$	$k_{21} = 5.14$
$m = 2$	$k_{02} = 5.52$	$k_{12} = 7.01$	$k_{22} = 8.42$

Due to the rectangular shape of the potential (16), we imply $V(z) = V_{1,2}$ within the corresponding limits and for $E^{(j)}$ we obtain (in dimensionless units)

$$E^{(j)} = E_{j,n_j l_j m_j} + V_j = \frac{1}{2}\left(\frac{\pi^2}{L_j^2}n_j^2 + \frac{k_{l_j m_j}^2}{R^2}\right) + V_j. \quad (18)$$

Figure 2(a) demonstrates the energy levels in accordance with (18) for two wells. As seen from Fig. 2(b), the spectral lines are degenerate in respect of l, m.

To calculate the tunneling rate we substitute (6) and (8) into (15b) and integrate it as

$$\kappa = -\frac{4\delta(l_1 - l_2)}{\sqrt{L_1 L_2}}\int_0^L V(z)\sin\left[\frac{\pi n_1}{L_1}z\right]\sin\left[\frac{\pi n_2}{L_2}(z - L_1 - d)\right]dz \times$$

$$C_1 C_2 \int_0^R J_{l_1}\left(\frac{k_{l_1 m_1} r}{R}\right) J_{l_2}\left(\frac{k_{l_2 m_2} r}{R}\right) dr, \quad (19)$$

where $L = L_1 + d + L_2 = 20$ nm is the full length of a micropillar. The delta function $\delta(l_1 - l_2)$ in (19) arises from (8a) and determines that the electron tunneling is allowed only between the levels with the same quantum number l. The integration on z and r in (19) is performed numerically with (17). For combinations of quantum numbers $n = 1,2,\ldots,6$; $l = 0,1,2$; $m = 1,2$ the strongest transitions (with the largest values of κ) are:

- $(n_2 = 2, l, m) \to (n_1 = 2, l, m)$ for $l_1 = l_2 \equiv l = 0,1,2$;

  $m_1 = m_2 \equiv m = 1,2$ with $\kappa = 0.8474$ eV and $E^{(1)} - E^{(2)} \approx 0.2545$ eV;

- $(n_2 = 3, l, m) \to (n_1 = 3, l, m)$ for $l_1 = l_2 \equiv l = 0,1,2$;

  $m_1 = m_2 \equiv m = 1,2$ with $\kappa = 0.4798$ eV and $E^{(1)} - E^{(2)} \approx 0.2352$ eV.

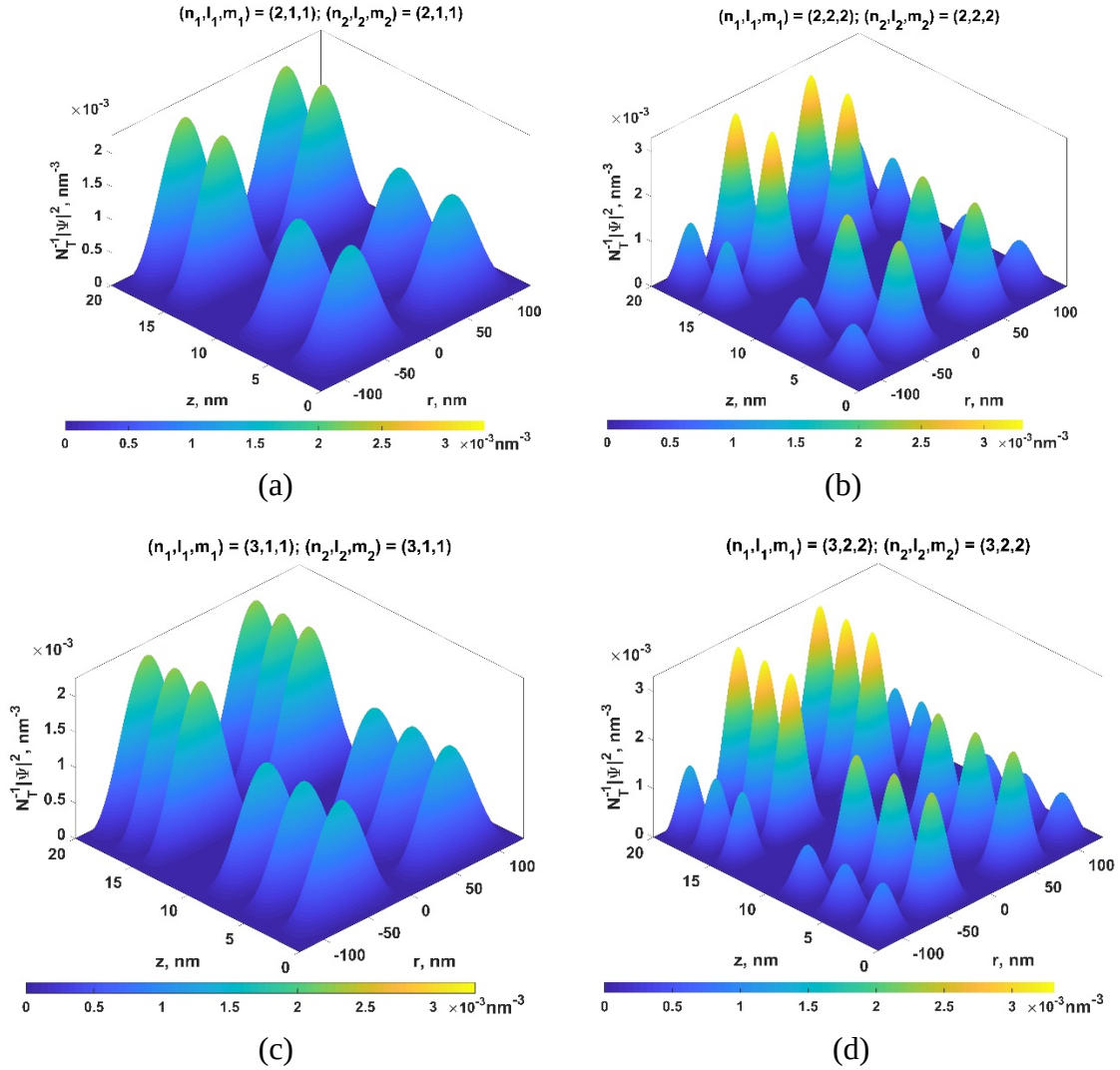

Fig. 3. (a-d) projections of the probability density distribution $|\Psi(\boldsymbol{r})|^2/N_T$ onto the micropillar diametrical section for the strongest transitions. The values of the quantum numbers are given in the plots

Figure 3 demonstrates the distributions of the wave function for strongest transitions occurring at the moment of time when $N_2 = N_1$, which we calculated as

$$\frac{|\Psi(\boldsymbol{r})|^2}{N_T} = \frac{1}{2}\left(\left|\Phi_1\left(\boldsymbol{r} + \frac{\boldsymbol{r}_0}{2}\right)\right|^2 + \left|\Phi_1\left(\boldsymbol{r} - \frac{\boldsymbol{r}_0}{2}\right)\right|^2\right), \quad (20)$$

where N_T is the total number of electrons in the conduction band; in (20) we also take into account (12). For clarity, Fig. 3 presents the projections of wave functions (20) onto the diametrical section of the micropillar (see Fig. 3(e)) in $z-r$ coordinates, expressed in nanometers.

4. Discussion

The tunneling current represents one of the important characteristics, which determine detector features. In particular, population difference between two wells determines the tunneling current $j(t) \propto \frac{d}{dt}(N_2 - N_1)$, where $N_j = \left|a_j\right|^2$. We substitute $a_j = \sqrt{N_j}e^{i\Theta_j}$ into (14) and then obtain ($\hbar = 1$) [24]:

$$j(t) \propto \left(\frac{d}{dt}N_2 - \frac{d}{dt}N_1\right) = -4\kappa\sqrt{N_1 N_2}\sin[\Theta], \quad (21a)$$

$$\frac{d}{dt}\Theta = E^{(1)} - E^{(2)} + \kappa\frac{N_1 - N_2}{\sqrt{N_1 N_2}}\cos[\Theta], \quad (21b)$$

where $\Theta = \Theta_2 - \Theta_1$ is the collective phase difference of the electrons in two wells. Finally, introducing population imbalance $\xi = (N_1 - N_2)/N_T$ we obtain:

$$\frac{j(t)}{N_T} \propto \dot{\xi} = -2\kappa\sqrt{1-\xi^2}\sin[\Theta], \quad (22a)$$

$$\dot{\Theta} = E^{(1)} - E^{(2)} + 2\kappa\frac{\xi}{\sqrt{1-\xi^2}}\cos[\Theta]. \quad (23b)$$

For example, let us examine the transition $(n_2 = 2, l, m) \rightarrow (n_1 = 2, l, m)$, $\kappa = 0.8474$ eV, $E^{(1)} - E^{(2)} \approx 0.2545$ eV for Eqs. (22). Suppose, at the initial moment of time $N_2/N_T = N_1/N_T = 0.5$, ($\xi = 0$) and $\Theta = 0$. Then, numerically solving the system of Eqs. (22), we obtain the dependence $j(t)$ shown in Fig. 4.

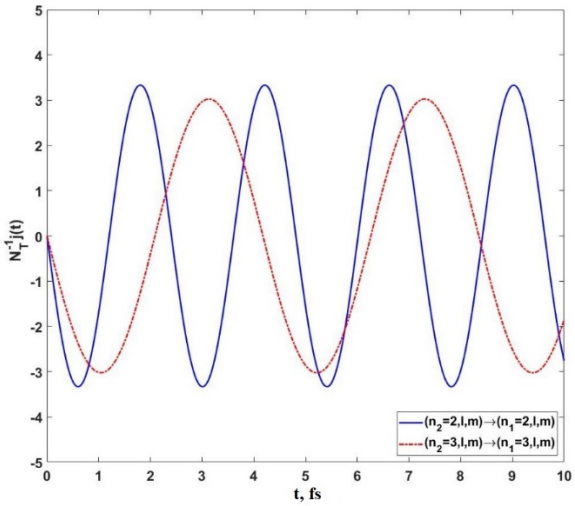

Fig. 4. Rabi-like oscillations of the tunneling current for the transition $(n_2 = 2, l, m) \rightarrow (n_1 = 2, l, m)$ with $\kappa = 0.8474$ eV and $E^{(1)} - E^{(2)} \approx 0.2545$ eV (the blue curve) and transition $(n_2 = 3, l, m) \rightarrow (n_1 = 3, l, m)$ with $\kappa = 0.4798$ eV and $E^{(1)} - E^{(2)} \approx 0.2352$ eV (the red curve); $l = 0,1,2$; $m = 1,2$

As seen from Fig. 4, in the absence of the external electric field, the tunneling current represents Rabi-like oscillations with a period of the order of femtoseconds [24]. Due to the energy difference $\Delta E = E^{(1)} - E^{(2)} > 0$ the electron transition, and thus the Rabi oscillations in Fig. 4, occurs under the absorption of a photon with energy $\hbar\omega_{ph} \approx \Delta E$. On the other hand, as seen from Fig. 4 the mean value of the photocurrent equals zero. Applying the external electric field (potential difference) to the micropillar in z direction we are able to shift the mean value of photo-current Rabi oscillations away from zero value. Again, photon

absorption remains necessary to obtain the photocurrent, which makes the considered micropillar heterostructure a photodetector.

References

[1] O'Brien JL, Furusawa A, Vuckovic J. Photonic quantum technologies. *Nature Photonics.* 2009;3(12): 687-695.
[2] Pirandola S. Advances in quantum cryptography. *Advances in Optics and Photonics.* 2020;4(12): 1012-1236.
[3] Gisin N, Thew R. Quantum communication. *Nature photonics.* 2007;1(3): 165-171.
[4] Michler P. *Quantum dots for quantum information technologies.* Berlin: Springer; 2017.
[5] Schlehahn A, Fischbach S, Schmidt R, Kaganskiy A, Strittmatter A, Rodt S. A stand-alone fiber-coupled single-photon source. *Scientific Reports.* 2018;8(1): 1.
[6] Mrowinski P, Musia A, Gawarecki K, Dusanowski HT, Srocka N. Excitonic complexes in mocvd-grown InGaAs/GaAs quantum dots emitting at telecom wavelengths. *Physical Review B.* 2018;100(11): 26772.
[7] Schnauber P, Schall J, Bounouar S, Hohne T, Park SI, Ryu G. Deterministic integration of quantum dots into on-chip multimode interference beam splitters using in situ electron beam lithography. *Nano Letters.* 2018;18(4): 2336.
[8] Carmele A, Reitzenstein S. Non-markovian features in semiconductor quantum optics: quantifying the role of phonons in experiment and theory. *Nanophotonics.* 2019;8(5): 655.
[9] Zolnacz K, Musia A, Srocka N, Grobe J, Schlösinger MJ, Schneider P. Method for direct coupling of a semiconductor quantum dot to an optical fiber for single-photon source applications. *Optics Express.* 2019;27(19): 26772.
[10] Hadfield RH. Single-photon detectors for optical quantum information applications. *Nature Photonics.* 2009;3(12): 696.
[11] Schlottmann E, Schicke D, Kruger F, Lingnau B, Schneider C, Höfling S. Stochastic polarization switching induced by optical injection in bimodal quantum-dot micropillar lasers. *Optics Express.* 2018;27(20): 28816.
[12] Jagsch ST, Trivino NV, Lohof F, Callsen G, Kalinowski S, Rousseau IM. A quantum optical study of thresholdless lasing features in high-β nitride nanobeam cavities. *Nature Communications.* 2018;9(1): 1.
[13] Kaganskiy A, Kreinberg S, Porte X, Reitzenstein S. Micropillar lasers with site-controlled quantum dots as active medium. *Optics Express.* 2019;6(4): 404.
[14] Jahnke F, Gies C, Abmann M, Bayer M, Leymann AM, Foerster A. Giant photon bunching, superradiant pulse emission and excitation trapping in quantum-dot nanolasers. *Nature communications.* 2016;7(1): 1.
[15] Kreinberg S, Porte X, Schicke D, Lingnau B, Schneider C, Höfling S. Mutual coupling and synchronization of optically coupled quantum-dot micropillar lasers at ultra-low light levels. *Nature Communications.* 2019;10(1): 1.
[16] Ceccarelli F, Acconcia G, Gulinatti A, Ghioni M, Rech I, Osellame R. Recent advances and future perspectives of single-photon avalanche diodes for quantum photonics application. *Advanced Quantum Technologies.* 2021;4(2): 2000102.
[17] Gangopadhyay S, Nag BR. Energy levels in three-dimensional quantum-confinement structures. *Nanotechnology.* 1997;8(1): 14.
[18] Gebhard T, Souza P, Alvarenga D, Parra-Murillo CA, Guimarães PSS, Unterrainer K, Pires MP, Vieira GS, Villas-Boas JM, Maialle MZ, Degani MH, Farinas PF, Studart N. InGaAs/InGaAlAs/InAs/InP very selective quantum dot infrared photodetector for 12 m. In: *2009 IEEE LEOS Annual Meeting Conference Proceedings.* IEEE; 2009. p.170.

[19] Holzinger S, Schneider C, Höfling S, Porte X, Reitzenstein S. Quantum-dot micropillar lasers subject to coherent time-delayed optical feedback from a short external cavity. *Scientific Reports.* 2019;9(1): 1.
[20] Holzinger S, Kreinberg S, Hokr BH, Schneider C, Höfling S, Chow WW. Determining the line width enhancement factor via optical feedback in quantum dot micropillar lasers. *Applied Physics Reviews.* 2018;26(24): 31363.
[21] Gangopadhyay S, Nag BR. Energy levels in three-dimensional quantum-confinement structures. *Nanotechnology.* 1997;8(1): 14.
[22] Raghavan S, Agrawal GP. Switching and self-trapping dynamics of Bose-Einstein solitons. *Journal of Modern Optics.* 2000;47(7): 1155.
[23] Landau LD, Lifshitz EM. *Quantum mechanics. Course of theoretical physics*. 1989. (In-Russian)
[24] Smerzi A, Fantoni S, Giovanazzi S, Shenoy SR. Quantum coherent atomic tunneling between two trapped Bose-Einstein condensates. *Physical Review Letters.* 1997;79(25): 4950.

THE AUTHORS

Tsarev D.V.
e-mail: dmitriy_93@mail.ru
ORCID: 0000-0002-9041-2708

Bazhenov A.Yu.
e-mail: b.a.y@mail.ru
ORCID: 0000-0002-7644-7568

Odnoblyudov M.A.
e-mail: maxim.odnoblyudov@spbstu.ru
ORCID: 0000-0003-3021-6892

Alodjants A.P.
e-mail: alexander_ap@list.ru
ORCID: 0000-0003-1247-2761